ADVANCED MATERIALS
www.advmat.de

Touch-Driven Bi-Chiral Superstructures for Nested Encryption of Multiplexed Optical Information

Rui Sun, Si-Jia Liu, Yi-Heng Zhang, Pei-Han Xu, Lin Zhu, Dong Zhu, Wen Chen, Yi-Ming Wang, Shi-Hui Ding, Shi-Jun Ge, Peng Chen, Bing-Yan Wei,* Jianlin Zhao,* and Yan-Qing Lu**

With the growing demand for data security, optical encryption has emerged as a promising solution due to its high-speed, parallel and low-power-consumption characteristics. However, most optical encryption methods rely on static structures involved with only few optical degrees of freedom (DOFs), resulting in simple encryption methods susceptible to attacks. Herein, a dynamic nested optical encryption scheme is proposed using a touch-driven bi-chiral cholesteric liquid crystal (CLC) superstructure, where relief-structured polymerized CLCs are combined with temperature-sensitive opposite-handed CLCs. Through delicate photopatterning and Bragg reflection engineering, independent geometric phases can be induced to the reflected light with orthogonal circular polarization and multiple wavelengths. Thus, various optical DOFs (wavelength, amplitude, and polarization) and environmental factors (temperature or human-device interaction) are encoded as different encryption dimensions. Based on the developed four-step encryption algorithm, the four-level nested encryption is demonstrated by multiplexing the plaintext and multilevel ciphertexts in structural colors, multicolored vectorial holography and their temperature-driven variations. The plaintext can be derived only through a specific order, with the final step completed by a human touch. This work advances the on-demand construction of chiral nanostructures, and offers a new paradigm for high-security and high-capacity optical informatics.

1. Introduction

With the emergence of the information era, industries such as finance and healthcare show increasing reliance on robust data protection, boosting the rapid evolution of encryption algorithms.[1,2] Early standards represented by the Data Encryption Standard (DES) employ a single key with a constant size to encrypt and decrypt data,[3] forming the foundation for modern techniques. Multi-DES further enhances the security by applying multiple encryption rounds with different keys.[4,5] This nested encryption scheme introduces greater complexity in the decryption, thereby making the system more resistant to attacks. However, optimizing encryption algorithms alone is no longer enough with the rapid rise of exhaustive search attacks. It is crucial to integrate other physical media into the encryption processes to prevent electronic-based cracking. In this context, optical encryption stands out as a competitive solution due to its high-speed, parallel, and low-power-consumption nature,[6–9] holding great potential for significantly enhancing the security in information storage and communication.

Optical encryption, which encrypts information by modulating various degrees of freedom (DOFs) of light,[10–13] has undergone rapid development in recent years. The holographic encryption can be achieved by controlling the amplitude, wavelength and polarization of light with artificial nanostructures.[14–18] Especially, using metasurfaces with subwavelength meta-atoms, simultaneous spin- and wavelength-multiplexed holography across the visible spectrum has been realized with high fidelity.[19–21] Besides, the structural color-based encryption is enabled by the angle- or wavelength-dependent responses of photonic crystals,[22,23] metal nanoparticles[24,25] and chiral polymers.[26–28] However, existing schemes usually rely on static optical structures involved with very limited optical DOFs, resulting in relatively simple encryption strategies that are vulnerable to attacks. In contrast, dynamic structures not only enable function switching[29–31] and external control,[32,33] but also allow more optical DOFs and active variations to be encoded as different encryption

R. Sun, S.-J. Liu, Y.-H. Zhang, L. Zhu, D. Zhu, W. Chen, Y.-M. Wang, S.-H. Ding, S.-J. Ge, P. Chen, Y.-Q. Lu
National Laboratory of Solid State Microstructures
Key Laboratory of Intelligent Optical Sensing and Manipulation
College of Engineering and Applied Sciences
and Collaborative Innovation Center of Advanced Microstructures
Nanjing University
Nanjing 210093, China
E-mail: chenpeng@nju.edu.cn; yqlu@nju.edu.cn
Y.-H. Zhang, P.-H. Xu, B.-Y. Wei, J. Zhao
Key Laboratory of Light Field Manipulation and Information Acquisition
Ministry of Industry and Information Technology
and Shaanxi Key Laboratory of Optical Information Technology
School of Physical Science and Technology
Northwestern Polytechnical University
Xi'an 710129, China
E-mail: wbyxz@nwpu.edu.cn; jlzhao@nwpu.edu.cn

DOI: 10.1002/adma.202513318

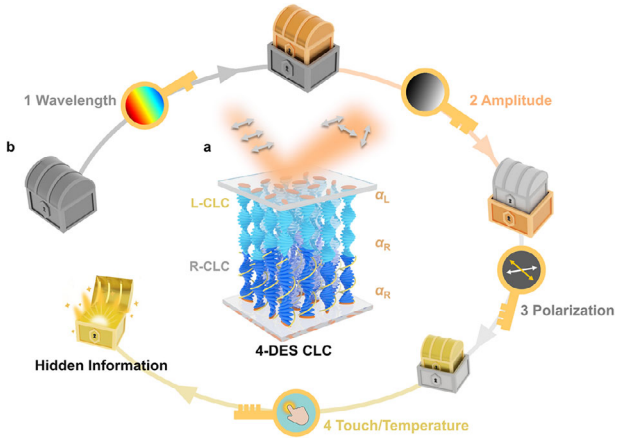

Figure 1. Schematic of the touch-driven dynamic nested optical encryption based on a bi-chiral liquid crystal superstructure. a) The bi-chiral liquid crystal superstructure (referred to as a 4-DES CLC due to its encryption capability), where the light blue rods represent the L-CLC and the dark blue rods represent the R-CLC, with their respective orientation angles denoted as α_L and α_R. When a polarized beam is incident (with the polarization direction indicated by the gray double-headed arrows), the far-field polarization distribution can be modulated by the bi-chiral superstructure. b) The nested multiplexed optical encryption mechanism, where the treasure boxes represent the multilevel encrypted ciphertexts and the keys represent distinct encryption dimensions. After decrypting one ciphertext with a key (dimension), another ciphertext appears, which requires further decryption. Ultimately, only by sequentially decrypting with four keys—wavelength, amplitude, polarization, and touch (temperature)—can the hidden information be retrieved.

dimensions. Among them, liquid crystals possess excellent dynamic response characteristics, enabling spin-isolated dynamic holography over a broadband range through integration with metasurfaces,[34] as well as tunable color-polarization separation using chiral liquid crystals.[35] Promisingly, such dynamic structures could incorporate environmental stimuli or even users' biometric characteristics[36,37] into the decryption process, which may enable effective authentication driven by human-device interaction. While existing dynamic schemes mainly focus on single-level optical encryption, it is urgent to explore a new platform that can integrate dynamic functionalities with multiple optical DOFs to further enhance the encryption security.

Cholesteric liquid crystals (CLCs), characterized by helically arranged molecules, not only excel in light control,[38–41] but also exhibit distinctive responsiveness to diverse external stimuli[42–45] (e.g., heat, electric/magnetic field, and light irradiation). In this work, we propose a dynamic nested optical encryption scheme based on touch-driven bi-chiral CLCs. Through a surface-initiated wash-out/refill process, polymerized right-handed CLCs (R-CLCs) and dynamic left-handed CLCs (L-CLCs) are integrated to form a hierarchical bi-chiral superstructure (**Figure 1a** (inner)). The R-CLCs feature a relief structure with space-variant helical pitches, while the L-CLCs are sensitive to temperature and thus responsive to human touch. Inspired by the multi-DES method, a four-step dynamic encryption algorithm (4-DES) is developed to encode wavelength, amplitude, polarization, and human touch as four encryption dimensions (Figure 1b (outer)). Only through a specific order can the information be correctly decrypted from structural colors and multicolored vectorial holography. Especially, the final step necessitates dynamic temperature tuning via human touch, further enhancing the information security. This work enriches the dynamic manipulation of chiral superstructures, and shows a promising method for high-security optical encryption and decryption.

2. Results

2.1. Principle of the Optical 4-DES Based on Bi-Chiral CLCs

The DES encryption can be formulated as $C = E_K(P)$,[3,4] where C is the ciphertext, P is the plaintext, and E_K denotes the encryption operation with the key K. Since DES uses only a single key, its encryption security can be compromised. Here, inspired by multi-DES, we propose a 4-DES optical encryption scheme to further enhance encryption security (Figure 1b). Four dimensions, including wavelength, amplitude, polarization, and touch/temperature, serve as the keys for the four-step nested encryption. Specifically, the encryption process for this 4-DES can be expressed as

$$C = E_{K_1}\left(E_{K_2}\left(E_{K_3}\left(E_{K_4}\left(P\right)\right)\right)\right) \tag{1}$$

Similarly, the decryption process reverses this operation by applying the keys in the reverse order:

$$P = D_{K_4}\left(D_{K_3}\left(D_{K_2}\left(D_{K_1}\left(C\right)\right)\right)\right) \tag{2}$$

In 4-DES, the decrypted result of one step becomes the ciphertext for the next decryption step. Only by sequentially using the four keys can the final hidden information be decrypted properly. Such nested encryption significantly enhances security by utilizing multi-dimensional keys, offering stronger protection against unauthorized access.

To realize the 4-DES optical encryption system, we propose a bi-chiral superstructure which combines a stabilized R-CLC layer and a dynamic L-CLC layer (Figure 1a). Using this structure, circularly polarized (CP) light that simultaneously matches the R-/L-CLC's chirality and photonic bandgap (PBG, wavelength range: $n_o p$ to $n_e p$) can be Bragg reflected and gain a geometric phase.[46–48] n_o and n_e are the ordinary and extraordinary refractive indices of liquid crystals, and p is the CLC helical pitch. Specifically, the polymerized R-CLC layer features helicoidal structures with space-variant heights and PBG, resulting in an uneven relief-structured surface. Meanwhile, the L-CLC layer exhibits thermal responsiveness, allowing its PBG to shift under temperature variation or human touch. Furthermore, by employing the multi-step photoalignment technology, the orientation angles of R-CLC and L-CLC (α_R and α_L) can be precisely manipulated, inducing the spin-decoupled and wavelength-selective CLC geometric phase. That is, the incident right/left circularly polarized (RCP/LCP) light can be respectively tailored by R-CLC and L-CLC and acquire the independent geometric phases of $+2\alpha_R$ and $-2\alpha_L$ only within their local PBG.

For light incident from the L-CLC side, the reflected light can be expressed as

$$\mathbf{E} = \begin{pmatrix} E_R \\ E_L \end{pmatrix} = \begin{pmatrix} A_R\left(x, y, \lambda\right) \cdot \exp\left(\mathrm{i}\left(2\alpha_R + \phi\left(\lambda\right)\right)\right) \\ A_L\left(T, \lambda\right) \cdot \exp\left(-\mathrm{i}2\alpha_L\right) \end{pmatrix} \tag{3}$$

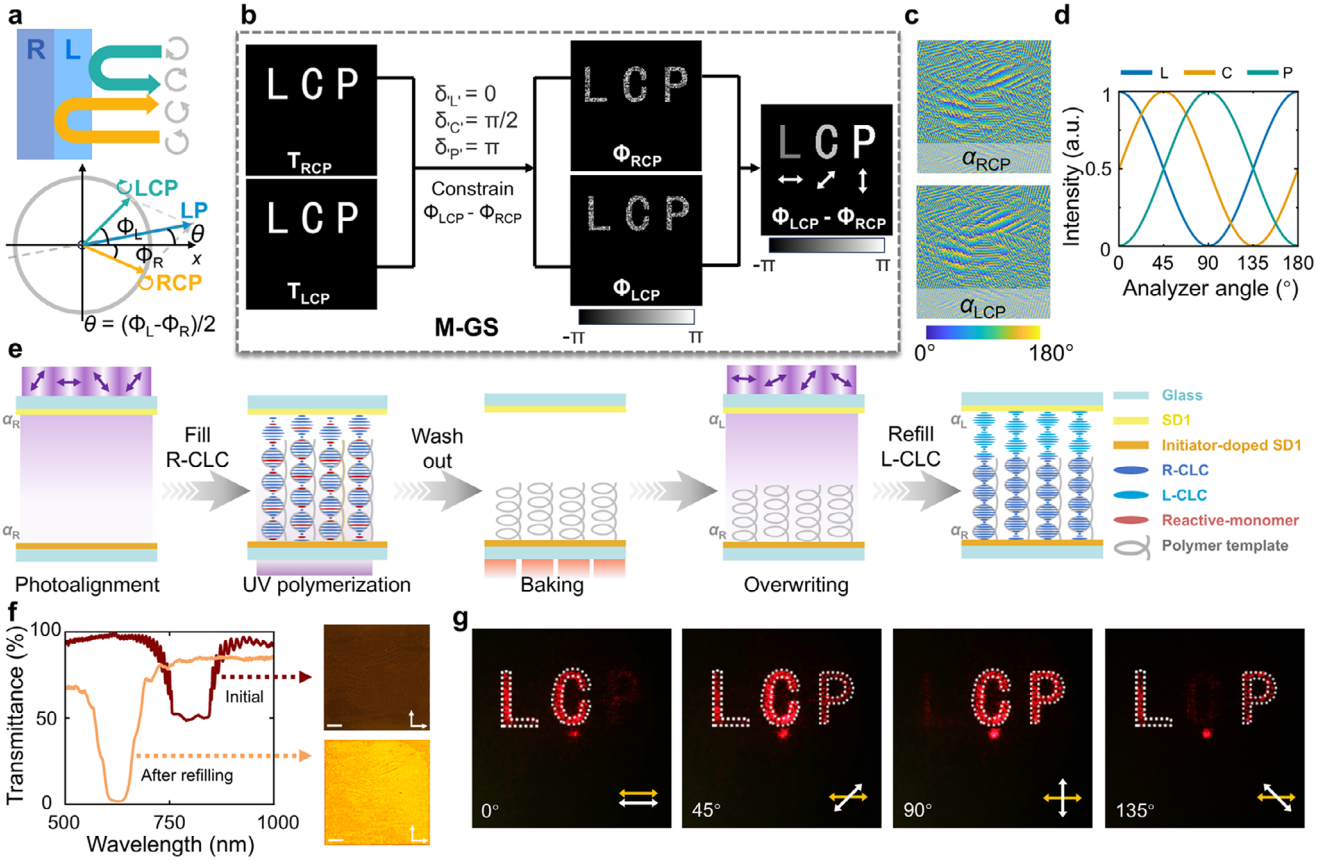

Figure 2. Design, fabrication, and characterization of the bi-chiral superstructure for polarization-empowered optical encryption. a) Principle of phase and polarization modulation via the bi-chiral hierarchical structure. The LCP light is reflected by the L-CLC layer, acquiring the phase Φ_L, while the RCP light is reflected by the R-CLC layer, obtaining a different phase Φ_R (upper). LP light is synthesized from the reflected LCP and RCP light, with its final polarization direction determined by $(\Phi_L - \Phi_R)/2$ (lower). b) Schematic of the modified Gerchberg-Saxton (M-GS) algorithm, where the target images for RCP and LCP are set as the same letters "LCP", with imposed phase difference constraints of 0 for "L", $\pi/2$ for "C", and π for "P". c) Orientation distribution generated by the M-GS algorithm after iterative optimization. d) Theoretical intensity curves of the letters "L", "C", and "P" at different analyzer angles. e) The surface-initiated wash-out/refill process. f) Polarized transmittance spectra and polarized optical micrographs at different fabrication stages. The white arrows depict the orthogonal polarizer and analyzer of the optical microscope. The scale bars represent 150 μm. g) Experimental results of "LCP" vectorial holography under different analyzer angles. Yellow and white arrows depict the polarizing and analyzing directions, respectively.

A_R and A_L represent the amplitudes of the RCP and LCP components, respectively, which are related to the spatial coordinates (x, y), wavelength λ, and temperature T. ϕ is a wavelength-dependent extra phase intrinsic to the bi-chiral superstructure. Specifically, according to the local PBG of R-CLC and L-CLC, A_R and A_L vary with the wavelength of light, forming the diverse Bragg reflection spectra and structural colors. The CLC orientation α_R/α_L can modulate the geometric phase distribution for RCP/LCP light, respectively, enabling the far-field amplitude shaping through holographic technologies. With linearly polarized (LP) incident light, the far-field polarization distribution can also be variously controlled by manipulating the phase difference between LCP and RCP light (**Figure** 2a). Moreover, the thermo- and touch-responsive L-CLC further enriches the dynamic characteristics of A_L under varying conditions. Overall, this bi-chiral superstructure simultaneously enables near-field structural colors, far-field vector light control, and dynamic thermal responses, making it a potential platform for the proposed 4-DES optical encryption.

2.2. Polarization-Empowered Holographic Optical Encryption

First, a modified Gerchberg-Saxton (M-GS) algorithm is designed to arbitrarily control the amplitude and polarization of holographic targets with the proposed bi-chiral superstructure. In our design, as shown in Figure 2b, the "LCP" letters are set as the target holographic image for both RCP and LCP light, but their phase difference $\Phi_{LCP} - \Phi_{RCP}$ is constrained to 0, $\pi/2$, and π for "L", "C", and "P", respectively. After iterative optimization, although the individual phases Φ_{LCP} and Φ_{RCP} appear random, their actual phase difference $(\Phi_{LCP} - \Phi_{RCP})$ approaches the desired values due to the phase constraints. Therefore, when RCP and LCP light spatially overlap in the far field, the "LCP" vectorial holography can be formed, where the polarization angles of the letters "L", "C", and "P" are 0°, 45°, and 90°, respectively (see more details in Figure S1 and Section S1, Supporting Information). The accordingly optimized orientations for R-CLC and L-CLC are illustrated in Figure 2c. Figure 2d presents the theoretical intensity curve of the holographic image after passing through

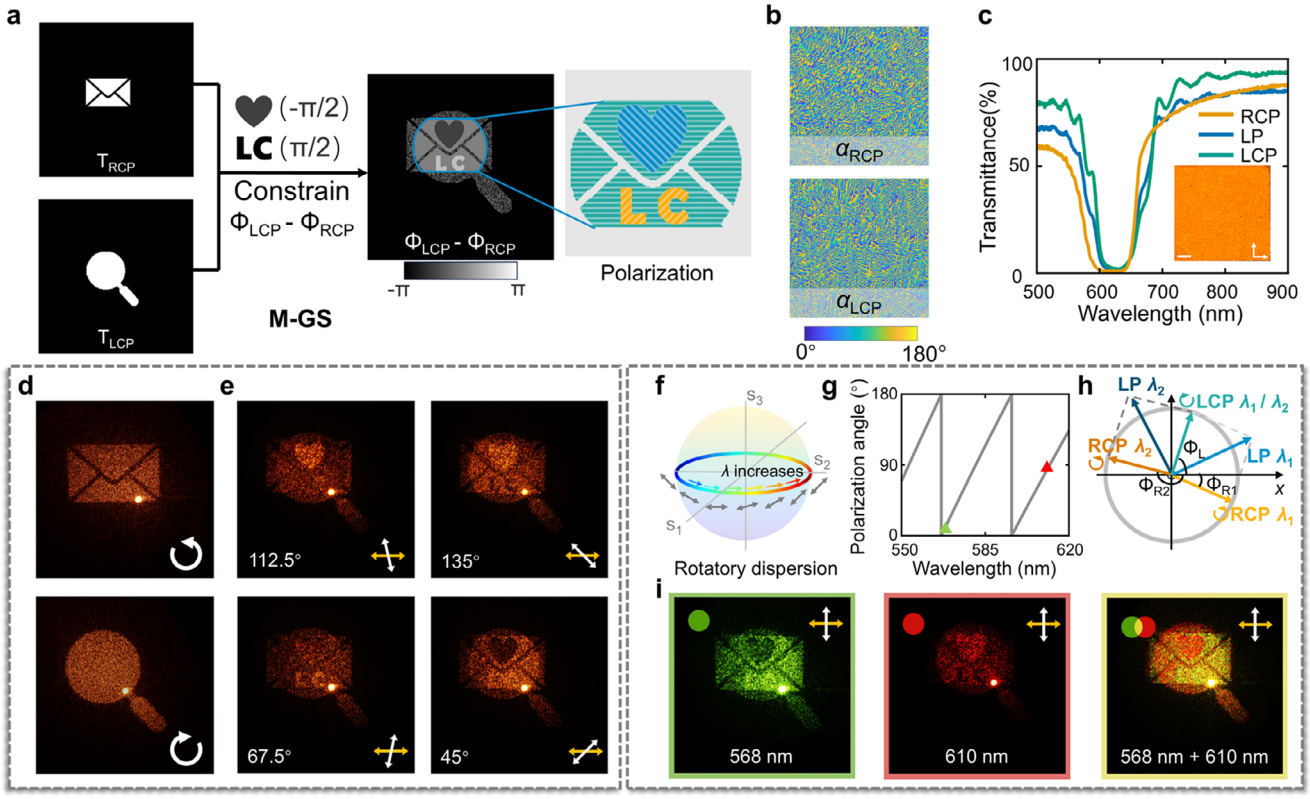

Figure 3. Polarization- and amplitude-involved optical encryption via vectorial holography. a) Configuration of the polarization- and amplitude-involved encryption based on the M-GS algorithm. b) Orientation distribution of the bi-chiral CLC generated by the M-GS algorithm. c) Polarized transmittance spectra and polarized optical micrographs of the fabricated bi-chiral superstructure. The scale bar represents 150 μm. d) Diffraction patterns reconstructed by RCP (upper) and LCP (lower) incidence. e) Decrypted images at different analyzer angles. f) Schematic illustration of the reflective optical rotatory dispersion (RORD) effect. g) Wavelength dependence of the reflected polarization angle calculated by the Berreman's 4 × 4 matrix method, where the green and red triangles indicate the two wavelengths selected in the experiment (see more details about the Berreman's 4 × 4 matrix method in Section S2, Supporting Information). h) Illustration of LP synthesis from LCP and RCP components under the influence of the RORD effect. i) Experimental decryption results at the wavelengths of 568 nm and 610 nm, along with their color mixing result.

an analyzer, where the intensity variations of the letters "L", "C", and "P" follow different cosine-squared curves (See theoretical image variations at different analyzer angles in Figure S2, Supporting Information).

As shown in Figure 2e, the bi-chiral superstructure was fabricated through a surface-initiated wash-out/refill process. First, the R-CLC with orientation α_R underwent polymerization, forming a right-handed polymer scaffold within the cell. Then, the unreacted molecules were washed with the acetone solution, leaving only a collapsed polymer scaffold.[49] After that, the orientation of the alignment layer was overwritten to α_L, and the L-CLC was refilled to form the bi-chiral CLC structure (see detailed fabrication process in Experimental Section). After the fabrication, the PBG center shifted from 800 nm to 632 nm, and finally achieved a high reflectance up to 93% for LP incident light (Figure 2f (left); Figure S3, Supporting Information), indicating a high efficiency for light manipulation. This PBG shift is also corroborated by the observed structural color variation at different fabrication stages (Figure 2f (right)). By illuminating the bi-chiral CLC with a LP laser from the L-CLC side (see the specific optical path in Figure S4, Supporting Information), the "LCP" vectorial holography is achieved (Figure 2g). Different letters are observed at various analyzer angles, including "LC" at 0°, "LCP" at 45°, "CP" at 90°, and "LP" at 135°, which is in good agreement with our theoretical design and the Malus' law.

Then, a polarization-empowered holographic encryption scheme is demonstrated using the bi-chiral CLC and the M-GS algorithm. The "envelope" and "magnifier" patterns serve as the holographic targets for RCP and LCP light, respectively (**Figure** 3a). In their overlapping region, the "heart" and "LC" patterns are embedded as encrypted information. $\Phi_{LCP} - \Phi_{RCP}$ is constrained to be $-\pi/2$, $\pi/2$, and 0 for each overlapping region (Figure 3a), resulting in polarization directions of -45°, 45°, and 0° under LP illumination. Figure 3b shows the orientation angles α_R and α_L optimized by the proposed M-GS algorithm. In experiment, following the fabrication process in Figure 2e, the encrypted bi-chiral hologram possesses an overlapped PBG (centered at 610 nm) and exhibits the orange structural color (Figure 3c). In the decryption process, only the "envelope" or "magnifier" pattern can be observed under CP light (Figure 3d). For LP incident light, the encoded information can only be decrypted at specific analyzer angles. The "heart" and "LC" patterns appear at 112.5° and 67.5°, respectively (Figure 3e; see other patterns in Figures S5 and S6, Supporting Information),

demonstrating the effectiveness of polarization- and amplitude-based encryption.

Moreover, utilizing the extra phase $\phi(\lambda)$ in Equation (3), the polarization-empowered holographic encryption can be further strengthened by a reflective optical rotatory dispersion effect. That is, when LP light is incident, the polarization direction of the reflected light varies with the wavelength (Figure 3f,g; see simulation details in Figure S7 and Section S2, Supporting Information), which is caused by the wavelength-dependent phase difference between LCP and RCP light (Figure 3h; see theoretical analysis in Section S3, Supporting Information). This effect necessitates the correct polarization-wavelength pair for decrypting the hidden information and enables the simultaneous retrieval of distinct plaintexts with polychromatic light. To demonstrate this, two wavelengths with a 90° polarization angle difference (568 nm and 610 nm, marked in Figure 3g) are used in the decryption process under a fixed analyzer. As shown in Figure 3i, a bright green "LC" pattern and a dark "heart" pattern are observed at 568 nm. Due to the 90° polarization variation, these patterns appear red with inverted brightness at 610 nm. The diffraction efficiency reaches a maximum value of 81% at 610 nm (see the experimental diffraction efficiency for all relevant working wavelengths in Figure S8, Supporting Information). Notably, when the two wavelengths of light are incident simultaneously, the green "LC" and red "heart" patterns appear at the same time, surrounded by some yellow color-mixing regions. See vivid image changing with different wavelength in Movie S1, Supporting Information. This phenomenon highlights the potential for multi-wavelength encryption, leading to richer encryption formats and higher information security.

2.3. Touch-Driven 4-DES Optical Encryption with Multiple DOFs

In addition to amplitude and polarization, the wavelength DOF and the dynamic responsiveness of CLCs are introduced as two new encryption dimensions to implement the dynamic 4-DES optical encryption. An amplitude constrained M-GS algorithm (**Figure** 4a) and a PBG patterning method (Figure 4b) are proposed to encode multiple optical DOFs. In the amplitude constrained M-GS algorithm (Figure 4a), two masks (Mask 1 and Mask 2) with complementary "laser" patterns are used as the amplitude constraints to calculate two individual groups of phase holograms, respectively. In the Mask 1 group, the holographic target for LCP is set as a "signboard" and a "polarizer", while that for RCP is a single "signboard". In their overlapping area, the polarization of a "touch" pattern is constrained to a LP direction different from its background. While in the Mask 2 group, the holographic targets for LCP and RCP are set as the same "treasure chest", with a "LC" pattern similarly constrained in their overlapping area. Then, the derived two groups of phase holograms are merged into two complete phase profiles for LCP and RCP, respectively. Accordingly, the CLC orientations α_{LCP} and α_{RCP} are obtained, which can simultaneously encode the amplitude and polarization DOFs through vectorial holography (more detailed encryption process can be found in Sections S4 and S5 and Figures S9 and S10, Supporting Information).

In our PBG patterning method (Figure 4b), Mask 1 and Mask 2 can be assigned to different wavelengths for R-CLC through the micro-scale structural color tailoring during the wash-out/refill process. Before the photoalignment of α_L, an additional UV exposure process is added to affect the rebound ability of the polymer template. Longer exposure time leads to weaker rebound ability, so the ultimate CLC pitch will be shorter and the PBG will shift toward a shorter wavelength (see detailed process in the Experimental Section). In our design, the patterns of Mask 1 and Mask 2 are exposed for different durations to achieve distinct Bragg bands. As shown in Figure 4c, the "laser" pattern appears in red and green structural colors with clear boundaries, effectively activating the wavelength DOF and thereby enriching the encrypted information.

Furthermore, the refilled L-CLC is carefully designed with an optimized ratio of E7 (nematic liquid crystal) and S811 (thermosensitive chiral dopant). This composition allows the sensitive pitch shortening of L-CLC when heated from room to body temperature (Figure 4d), thus enabling the touch-driven PBG shift. As the temperature increases from 27.0 °C to 34.0 °C, the color of L-CLC changes from red to green (Figure 4e), while the R-CLC remains stable (Figure 4c). The response time of the L-CLC was measured to be 17 s (see more details in Figure S11 and Movie S2, Supporting Information). As shown in Figure 4f, the reflection band of L-CLC precisely overlaps with the red region of R-CLC at 26.0 °C and gradually blue-shifts with the rise of temperature (see R-/L-CLCs with overlapped red regions in Movie S3, Supporting Information). At 34.0 °C, its PBG center shifts to ≈530 nm, overlapping with the green region of R-CLC (see more details in Figures S12 and S13, Supporting Information). Only when the PBGs of opposite-handed CLCs overlap can the vectorial holography be generated. Therefore, the temperature can be encoded as an additional encryption dimension. It can be altered by human touch to achieve varying Bragg band overlaps, enabling the dynamic switching of vectorial holography from the "touch" sign to the "LC" pattern.

Figure 5 presents the four-step nested decryption process of the 4-DES CLC. The macrograph of the fabricated 4-DES CLC is shown in Figure 5a, where each structural area occupies only 1.04 mm^2. Four keys need to be used sequentially to decrypt its encrypted information. First, since the micro-scale structural colors of the R-CLC are invisible to the naked eyes, a microscope is required to observe the embedded information in the wavelength DOF (K_1: Wavelength). A "laser" pattern in red and green structural colors is decrypted (C_1; Figure 5b), implying the need for both red and green lasers in the next decryption step. Second, the 4-DES CLC is simultaneously illuminated by 633 nm and 532 nm lasers to reconstruct a holographic image (K_2: Amplitude). Since the L-CLC PBG falls within the red spectral range at room temperature, some red holographic patterns can be observed in the far field (Figure 5c), among which the "polarizer" pattern indicates the need for polarization analysis (C_2). Thirdly, when an analyzer is added (K_3: Polarization), a "touch" sign is revealed on the "signboard" pattern (C_3; Figure 5d), which implies the need for human touch. Finally, upon touching (K_4: Touch), the temperature of the 4-DES CLC approaches the body temperature, causing the L-CLC PBG to shift to the green spectral range. From the dynamic change of the multicolored vectorial holography (Figure 5e), the final information—a green "LC" pattern (P)—is ultimately decrypted (see more details in Section 5 and Figure S10, Supporting Information). This decryption process

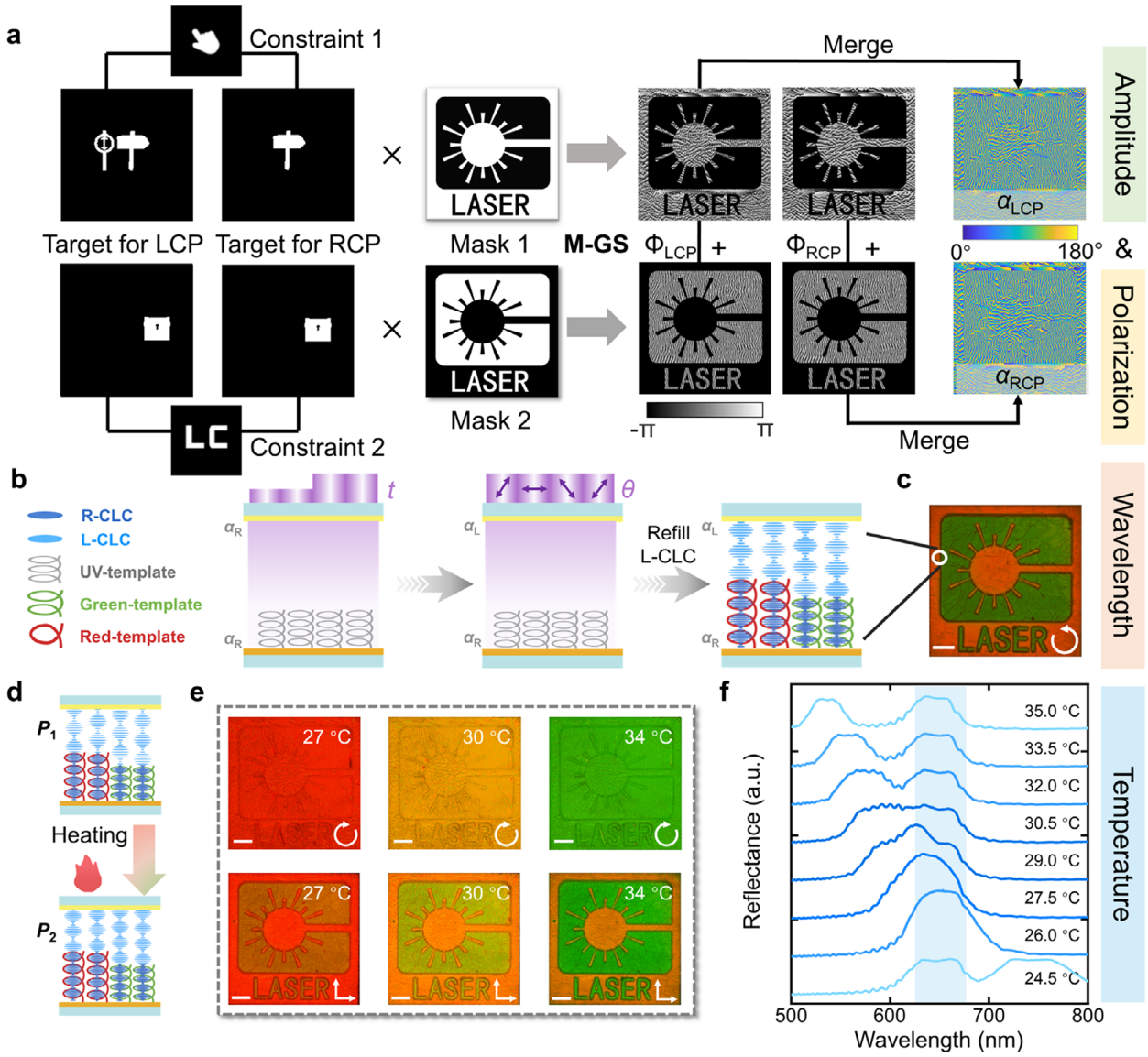

Figure 4. Dynamic 4-DES optical encryption involving the amplitude, polarization, wavelength of light, and the temperature. a) Configuration of the M-GS algorithm with amplitude constraints. b) PBG patterning process of the bi-chiral CLC, where the ultimate PBG of R-CLC is affected by the UV exposure duration *t*. c) Optical micrograph of the relief-structured R-CLC polymer template with RCP incidence. d) Schematic of the temperature-responsive dynamic pitch variation in the refilled L-CLC layer. Upon heating, the L-CLC pitch shortens from P_1 to P_2, resulting in a blue-shift of its PBG, while the R-CLC pitch remains fixed. e) Micrographs of the 4-DES CLC under LCP (upper) and LP (lower) incidence at varying temperatures. f) Evolution of the reflection spectra of the 4-DES bi-chiral CLC at different temperatures (measured within the red region of R-CLC). The blue block marks the fixed reflection band of the red region of R-CLC. All scale bars represent 150 μm.

introduces the concept of human-device interaction, significantly enhancing the security and interactivity of optical encryption.

3. Discussion

By integrating multiple optical DOFs with human-device interaction, the proposed 4-DES bi-chiral CLC greatly increases the data capacity and enhances the information security. To further expand its capacity, different degrees of color mixing (Figures S14 and S15, Supporting Information) can be introduced as an additional encryption dimension, thanks to the thermal tunability of the refilled CLCs. Furthermore, the current study can be extended to the full visible spectrum through optimization of the exposure process (see more details in Figure S16, Supporting Information) and introduction of large-birefringence liquid crystals, oblique helicoidal cholesterics,[50] or other thermally tunable CLCs.[35] Such spectral expansion would enhance their practical applications, particularly in advanced optical communications and information security systems. In addition to the temperature sensitivity demonstrated here, the active CLC layer can also be light-, electric- and humidity-sensitive,[51,52] which is promising to link the system to more dynamic dimensions. Moreover, by applying

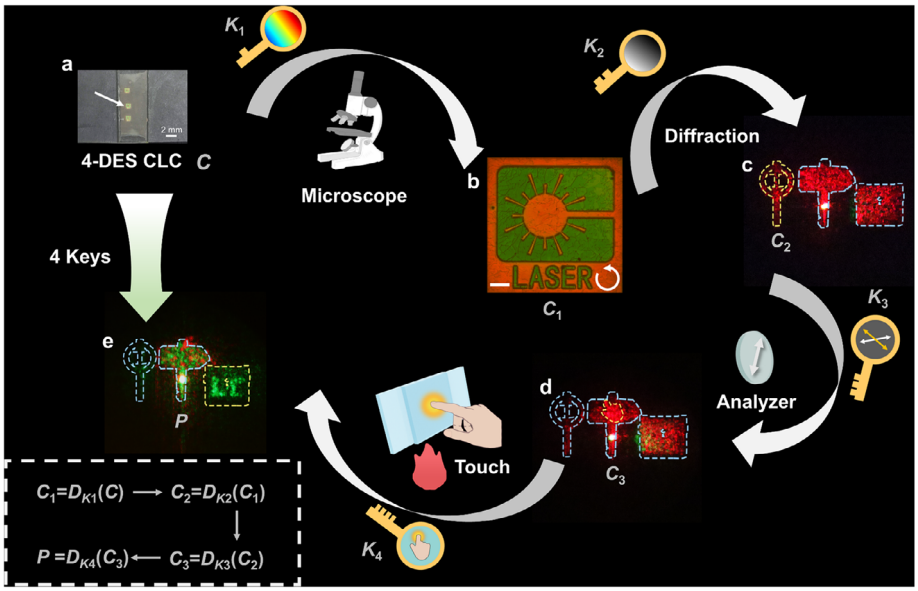

Figure 5. Touch-driven nested optical decryption of the 4-DES CLC. a) Macrograph (C) of the fabricated 4-DES CLC. The scale bar represents 2 mm. b) Micrograph of the 4-DES CLC with RCP incidence (C_1). The scale bar represents 150 µm. c) The decrypted holographic image, where the yellow-bordered region represents a "polarizer" pattern (C_2). d) The decrypted holographic image after an analyzer, with the yellow-bordered region highlighting a "touch" pattern (C_3). e) The decrypted holographic image after touching, where the green "LC" letters in the yellow-bordered area represent the final hidden information (P).

a second round of washing, overwriting and refilling, new optical information can be encrypted into the same CLC sample, allowing for recyclable and reprogrammable processing.

In summary, we have proposed and demonstrated a dynamic nested optical encryption scheme based on a touch-driven bi-chiral superstructure. A 4-DES CLC was created through a surface-initiated wash-out/refill process and a multi-step photopatterning technique. A total of six optical DOFs are efficiently manipulated, including amplitude, phase, polarization, wavelength, space, and temporal variation. Through engineering the space-variant PBG of R-CLC, the wavelength DOF is introduced as the first encryption dimension. Amplitude and polarization DOFs, as the second and third dimensions, are simultaneously encoded in vectorial holography by the circular-polarization-dependent phase modulation of bi-chiral CLCs. Furthermore, dynamic CLCs with thermal responsiveness are employed to incorporate human touch as the fourth encryption dimension. This nested encryption strategy has achieved four-dimensional optical multiplexing in terms of near/far field, polarization, wavelength, and temperature. This work promotes the construction strategies of active chiral nanostructures, and provides a multifunctional paradigm for smart authentication and secure optical information processing.

4. Experimental Section

Materials: The photoalignment agent SD1 (DIC, Japan) is dissolved in DMF at a concentration of 0.35 wt% to prepare the SD1 solution. The photoinitiator-doped SD1 solution is obtained by mixing the SD1 solution with 0.15 wt% diphenyl ketone. Under UV exposure, SD1 molecules tend to reorient perpendicularly to the UV linear polarization direction, thereby guiding the LC molecules to align parallel to them. The initial R-CLC mixture for polarization encryption and vectorial holography consists of nematic liquid crystal (LC) E7 (HCCH, China), right-handed chiral dopant R5011 (HCCH, China), and LC reactive monomer RM257 (HCCH, China) at a weight ratio of 78.1:1.9:20. The initial mixture for 4-DES encryption is prepared with a weight ratio of 78.4:1.6:20. The refilled L-CLC used for polarization encryption and vectorial holography consists of nematic LC E7 and left-handed chiral dopant S5011 (HCCH, China) at a weight ratio of 97.46:2.54. In contrast, the L-CLC for 4-DES encryption is composed of nematic LC E7 and thermosensitive chiral dopant S811 (HCCH, China) at a weight ratio of 74.3:25.7, which is carefully designed to accommodate the required temperature variations. The chemical structures of SD1, diphenyl ketone, RM257, R5011/S5011 and S811 are provided in Figure S17, Supporting Information.

Sample Fabrication: After UV-Ozone treatment, the ITO glass substrates were spin-coated with either SD1 solution or photoinitiator-doped SD1 solution and cured at 100 °C for 10 min to form an alignment layer. Then, a photoinitiator-free substrate was assembled with a photoinitiator-doped substrate using a 15-µm spacer/glue mixture along the upper and lower edges, forming an empty LC cell. Then, a surface-initiated wash-out/refill process was implemented (Figure 2e). First, a multi-step partly overlapping exposure process was conducted using a digital micromirror device (DMD)-based photopatterning system to achieve patterned photoalignment of the SD1 layer.[38] After that, the R-CLC mixture was filled into the cell at 80 °C. During polymerization, the cell was exposed to non-polarized UV light (365 nm, 4.6 mW cm^{-2}) for 15 min from the photoinitiator-doped side. Subsequently, the cell was immersed in acetone for 12 h to remove the unreacted molecules, leaving only a shrunk polymer scaffold that preserved the initial alignment and chirality. To engineer the final PBG, the shrunk scaffold was baked at 100 °C for 8 min for the polarization- and amplitude-involved encryption. While for the 4-DES encryption, a photopatterning process (365 nm, 158 mW cm^{-2}) with space-variant exposure time t was applied to the scaffold to form a relief-structured template, allowing the precise control over the final PBG distribution of R-CLC (Figure 4b). In general, higher-dose exposure weakens the rebound ability of the polymer scaffold, shortens the R-CLC pitch, and results in a bluer structural color. Afterward, a second polarized photopatterning step was performed to overwrite the alignment of SD1. Last, after

refilling with L-CLC, the L-CLC molecules were guided by the overwritten SD1 layer, forming the required bi-chiral CLC superstructure.

Characterizations: All data were measured at room temperature unless otherwise specified. All micrographs were captured using a polarized optical microscope (Ci-POL, Nikon, Japan). For the individual observation of the scaffold layer (R-CLC) and the refilled layer (L-CLC), an achromatic quarter-wave plate (AWP20Q-T2Q, JCOPTIX, China) was added to the microscopy system to control the incident polarization, while all other observations were conducted under crossed polarizers. The transmittance and reflectance spectra were measured using a spectrometer (PG2000-Pro-EX, Ideaoptics, China) with a halogen light source (iDH2000H-HP, Ideaoptics, China). Precise temperature control was achieved during the experiment using a hot stage (LTS120E, Linkam, UK). A supercontinuum fiber laser (SuperK EVO, NKT Photonics, Denmark) was used to generate light of different wavelengths, which was further filtered by a multi-channel acousto-optic tunable filter (SuperK SELECT, NKT Photonics, Denmark). The incident polarization was controlled using an achromatic polarizer (OPP-WG20, JCOPTIX, China) and the achromatic quarter-wave plate, and the reflected light was optionally filtered with an analyzer. Due to the influence of the additional phase difference, the polarizer angle corresponding was defined to the appearance of the 0° theoretical pattern as 0°. The far-field holographic images were projected onto a screen positioned 50 cm away from the sample and captured using a visible digital camera (EOS M50m2, Canon, Japan). The diffraction efficiency is defined as $\eta = (I_h - I_0) / I_r$, where I_h denotes the total intensity of the holographic pattern, I_0 represents the zeroth-order intensity, and I_r is the total intensity reflected from the bi-chiral CLC. Additionally, the optical power of UV exposure was precisely measured using a digital optical power meter (PM100D, Thorlabs, USA) to ensure accurate control of the exposure dosage.

Supporting Information

Supporting Information is available from the Wiley Online Library or from the author.

Acknowledgements

R.S. and S.J.L. contributed equally to this work. This work was supported by the National Natural Science Foundation of China (NSFC) (Nos. 62222507, T2488302, 62175101, 12374279, and 624B2065), the Fundamental Research Funds for the Central Universities (No. 021314380273), and the Program for Outstanding PhD Candidates of Nanjing University (No. 2025A13).

Conflict of Interest

The authors declare no conflict of interest.

Data Availability Statement

The data that support the findings of this study are available from the corresponding author upon reasonable request.

Keywords

chiral nanostructures, holography, liquid crystals, optical encryption, optical multiplexing

Received: July 11, 2025
Revised: September 28, 2025
Published online:

[1] E. Waks, K. Inoue, C. Santori, D. Fattal, J. Vuckovic, G. S. Solomon, Y. Yamamoto, *Nature* **2002**, *420*, 762.
[2] D. Boneh, M. Franklin, *SIAM J. Comput.* **2003**, *32*, 586.
[3] D. Coopersmith, *IBM J. Res. Dev.* **1994**, *38*, 243.
[4] J. Katz, Y. Lindell, *Introduction to modern cryptography*, Chapman and hall/CRC, Florida US **2020**.
[5] B. Schneier. *Applied cryptography second edition*, Wiley, New Jersey **1996**.
[6] Z. Niu, Y. Xie, G. Xu, C. Dai, H. Yang, C. Zeng, M. Shi, L. Li, G. Pu, W. Hu, L. Yi, *Natl. Sci. Rev.* **2025**, *12*, nwaf112.
[7] S. Nocentini, U. Ruhrmair, M. Barni, D. S. Wiersma, F. Riboli, *Nat. Mater.* **2024**, *23*, 369.
[8] P. Refregier, B. Javidi, *Opt. Lett.* **1995**, *20*, 767.
[9] J. Ahn, T. Park, T. W. Kang, S. G. Im, H. Seo, B. H. Kim, S. J. Kwon, S. J. Oh, *Sci. Adv.* **2025**, *11*, 10.
[10] S. Wan, K. Qu, Y. Shi, Z. Li, Z. Wang, C. Dai, J. Tang, Z. Li, *ACS Nano* **2024**, *18*, 18693.
[11] X. Fang, H. Ren, M. Gu, *Nat. Photonics* **2019**, *14*, 102.
[12] S. Sun, Y. Gou, T. J. Cui, H. F. Ma, *PhotoniX* **2024**, *5*, 38.
[13] X. Guo, P. Li, J. Zhong, D. Wen, B. Wei, S. Liu, S. Qi, J. Zhao, *Nat. Commun.* **2022**, *13*, 6687.
[14] C. Xu, R. Zhao, X. Zhang, S. Zhang, X. Li, G. Geng, J. Li, X. Li, Y. Wang, L. Huang, *eLight* **2024**, *4*, 9.
[15] H. S. Khaliq, A. Nauman, J. W. Lee, H. R. Kim, *Adv. Opt. Mater.* **2023**, *11*, 2300644.
[16] B. Xiong, Y. Liu, Y. H. Xu, L. Deng, C. W. Chen, J. N. Wang, R. W. Peng, Y. Lai, Y. M. Liu, M. Wang, *Science* **2023**, *379*, 294.
[17] X. Sui, Z. He, D. Chu, L. Cao, *Light Sci. Appl.* **2024**, *13*, 158.
[18] S. J. Liu, L. Zhu, Y. H. Zhang, W. Chen, D. Zhu, P. Chen, Y. Q. Lu, *Adv. Mater.* **2023**, *35*, 2301714.
[19] A. Asad, J. Seong, H. S. Khaliq, J. W. Lee, Y. Jeon, H. Cabrera, M. Q. Mehmood, L. Gao, H. R. Kim, J. Rho, *Adv. Funct. Mater.* **2024**, *34*, 2402744.
[20] Z. Liu, H. Gao, T. Ma, V. Ray, N. Liu, X. Zhang, L. J. Guo, C. Zhang, *eLight* **2024**, *4*, 7.
[21] Z. Zhao, Z. Wang, Y. Shi, S. Wan, Z. Li, *Adv. Mater.* **2025**, *37*, 2419322.
[22] X. Wen, K. Zhang, B. Wu, G. Chen, N. Zheng, J. Wu, X. Yang, T. Xie, Q. Zhao, *Nat. Commun.* **2025**, *16*, 2830.
[23] Y. Zhao, M. Zhang, Z. Wang, H. Li, Y. Hao, Y. Chen, L. Jiang, Y. Wu, S. Q. Zang, Y. Song, *Nat. Commun.* **2025**, *16*, 3316.
[24] Y. Bao, Y. Yu, H. Xu, C. Guo, J. Li, S. Sun, Z. K. Zhou, C. W. Qiu, X. H. Wang, *Light Sci. Appl.* **2019**, *8*, 95.
[25] M. Song, L. Feng, P. Huo, M. Liu, C. Huang, F. Yan, Y. Q. Lu, T. Xu, *Nat. Nanotechnol.* **2023**, *18*, 71.
[26] Y. Dong, H. Wu, J. Liu, S. Zheng, B. Liang, C. Zhang, Y. Ling, X. Wu, J. Chen, X. Yu, S. Feng, W. Huang, *Adv. Mater.* **2024**, *36*, 2401294.
[27] W. Yang, C. Zheng, L. Sun, Z. Bie, Y. Yue, X. Li, W. Sun, T. Ikeda, J. Wang, L. Jiang, *Adv. Mater.* **2025**, *37*, 2411988.
[28] M. Zhang, Q. Guo, Z. Li, Y. Zhou, S. Zhao, Z. Tong, Y. Wang, G. Li, S. Jin, M. Zhu, T. Zhuang, S. H. Yu, *Sci. Adv.* **2023**, *9*, adi9944.
[29] I. Nys, B. Berteloot, K. Neyts, *Adv. Opt. Mater.* **2022**, *10*, 2201289.
[30] C. Peng, C. Xu, W. Hu, *Chin. Opt. Lett.* **2024**, *22*, 053301.
[31] Z. Feng, J. Li, P. Yang, X. Xu, D. Wang, J. Li, C. Zhang, J. Li, H. Zhang, G. Zou, X. Chen, *Nat. Commun.* **2025**, *16*, 2264.
[32] Z. Y. Bie, W. J. Yang, Y. J. Chen, C. L. Zheng, T. Ikeda, J. X. Wang, L. Jiang, *Adv. Funct. Mater.* **2025**, *36*, 2424107.
[33] Y. H. Zhang, P. Chen, C. T. Xu, L. Zhu, X. Y. Wang, S. J. Ge, W. Hu, Y. Q. Lu, *ACS Photonics* **2022**, *9*, 1050.
[34] A. Asad, J. Kim, H. S. Khaliq, N. Mahmood, J. Akbar, M. T. S. Chani, Y. Kim, D. Jeon, M. Zubair, M. Q. Mehmood, Y. Massoud, J. Rho, *Nanoscale Horiz.* **2023**, *8*, 759.
[35] C. Yun, S. Nam, H. Kim, W. Jung, S. S. Choi, *ACS Appl. Mater. Interfaces* **2025**, *17*, 12532.

[36] Z. Wang, Z. Li, C. Wan, S. Wan, C. Dai, G. Zheng, Z. Li, *ACS Nano* **2025**, *19*, 1286.
[37] W. Zhu, B. Chen, D. Peng, *Sci. Bull.* **2024**, *69*, 2807.
[38] P. Chen, B. Y. Wei, W. Hu, Y. Q. Lu, *Adv. Mater.* **2020**, *32*, 1903665.
[39] H. K. Bisoyi, Q. Li, *Chem. Rev.* **2021**, *122*, 4887.
[40] R. Sun, S. Liu, P. Chen, Y. Lu, *Chin. J. Liq. Cryst. Disp.* **2024**, *39*, 1657.
[41] S. A. Jiang, C. C. Lai, Y. S. Zhang, J. D. Lin, W. C. Lin, X. L. Hsieh, C. R. Lee, *Adv. Opt. Mater.* **2021**, *9*, 2100746.
[42] Y. H. Zhang, S. H. Ding, Y. M. Wang, W. Chen, D. Zhu, S. J. Ge, P. Chen, Y. Q. Lu, *Nano Lett.* **2025**, *25*, 5c01480.
[43] B. Liu, C. L. Yuan, H. L. Hu, H. Wang, Y. W. Zhu, P. Z. Sun, Z. Y. Li, Z. G. Zheng, Q. Li, *Nat. Commun.* **2022**, *13*, 2712.
[44] M. C. Yeh, S. H. Yang, W. Lee, *J. Mol. Liq.* **2019**, *296*, 112082.
[45] P. Chen, L. L. Ma, W. Hu, Z. X. Shen, H. K. Bisoyi, S. B. Wu, S. J. Ge, Q. Li, Y. Q. Lu, *Nat. Commun.* **2019**, *10*, 2518.
[46] J. Kobashi, H. Yoshida, M. Ozaki, *Nat. Photonics* **2016**, *10*, 389.
[47] R. Barboza, U. Bortolozzo, M. G. Clerc, S. Residori, *Phys. Rev. Lett.* **2016**, *117*, 053903.
[48] M. Rafayelyan, G. Tkachenko, E. Brasselet, *Phys. Rev. Lett.* **2016**, *116*, 253902.
[49] L. Zhu, Y. Zhang, S. Ge, P. Chen, Y. Lu, *Chin. Opt. Lett.* **2024**, *22*, 061601.
[50] J. Kim, J. H. Im, S. So, Y. Choi, H. Kang, B. Lim, M. Lee, Y. K. Kim, J. Rho, *Adv. Mater.* **2024**, *36*, 2311785.
[51] D. Ahn, M. Lee, W. Kim, Y. K. Lee, J. Y. Lee, G. Y. Jung, H. Choi, Y. Yoon, H. S. Song, H. Lee, M. Seo, J. Min, Y. Pak, *Adv. Sci.* **2025**, *12*, 2412139.
[52] J. Yoon, C. Jung, J. Kim, J. Rho, H. Lee, *Nat. Commun.* **2024**, *15*, 6470.